JOURNAL OF MULTIDISCIPLINARY SCIENTIFIC KNOWLEDGE

Vol. 01, Issue. 02, June, 2026

Synergistic Recovery of Platinum Group Metals and Valuable Base Metals from Supergene Oxidized Ores via an Integrated Beneficiation–Hydrometallurgy Process

Sabelosami D. Malunga[1], O. N. Maliyon[2], E. Ticharwa[3]

Received:- 03/05/2026, Revised:- 12/06/2026, Accepted:- 20/06/2026, Published:- 27/06/2026

Abstract

Supergene oxidized ore bodies, which contain high-grade sulfide Platinum Group Metal (PGM) ore, are being increasingly explored for viable alternatives, as a result of depletion in the former reserves. There are more than 500 million metric tonnes of such oxidized reserves in the Great Dyke of Zimbabwe, but their exploitation has been hindered by the poor metallurgical performance of conventional flotation and pyrometallurgical processes. Weathering converts primary sulfide minerals into iron oxyhydroxides and silica passivating coatings and clay phases that inhibit mineral surface recovery of PGMs by less than 55%. In this study, an integrated five-stage beneficiation-hydrometallurgical flowsheet was developed and optimised experimentally using a bulk sample of 100 kg of an oxidized PGM ore, obtained from Karo Platinum Mine, Zimbabwe with certified grade of 2.667 g/t 3E; 1.695 g/t Pt, 0.476 g/t Pd, 0.496 g/t Au. The processing flowsheet included comminution to P_0 = 75 μm, Low-Intensity Magnetic Separation (LIMS) to reject the chromite, dilute H_2SO_4 acid scrubbing to remove the oxide coating, NaHS sulfidization to activate the surface, rougher froth flotation to concentrate the mineral (3E recovery 80.3%, 3E concentrate 28.64 g/t), cyanide gold leaching (Au recovery 88%), and oxidative chloride leaching (6 M HCl–H_2O_2, 120 min). This integrated flowsheet yielded an overall compound 3E recovery of 65.6%, a significant improvement over the recovery rate of less than 55% which was possible by conventional methods. A steady state process design was carried out at 100 t/h throughput which confirmed the technical viability of the proposed circuit.

Keywords: PGM; oxidized ore; LIMS; sulfidization; flotation; chloride leaching; process design; Great Dyke; Zimbabwe

[1*]Department of Chemical and Process Systems Engineering, School of Engineering and Technology, Harare Institute of Technology (HIT), Harare, Zimbabwe, h240747j@hit.ac.zw, +263 786 726 569
[2,3]Department of Chemical and Process Systems Engineering, School of Engineering and Technology, Harare Institute of Technology (HIT), Harare, Zimbabwe

Corresponding Author: Sabelosami D. Malunga

1. Introduction

The Platinum Group Metals (PGMs)—platinum (Pt), palladium (Pd), rhodium (Rh), ruthenium (Ru), iridium (Ir), and osmium (Os)—are among the most critical materials in the modern economy, especially for the development of various industries. Their outstanding catalytic, thermal and electrochemical characteristics are used in automotive catalytic converters, hydrogen fuel cells, petroleum refining, biomedical devices, and electronic components. Demand for PGMs remains on the rise as the world increasingly pursues decarbonisation policy and looks to hydrogen energy infrastructure to be deployed. The reserves of PGMs known worldwide are hosted by the Bushveld Igneous Complex of South Africa and the Great Dyke of Zimbabwe (Becker, 2021; Oberthür, 2018).

They are present in primary mineralization as separate phases such as sulfide, arsenide, and alloy (cooperite, PtS; sperrylite, $PtAs_2$; braggite, (Pt, Pd, Ni)S) that are finely disseminated in base metal sulfide matrices. Sulfide ores are traditionally processed using circuits that achieve recoveries in excess of 80% based on the natural hydrophobicity of sulfide surfaces in froth flotation. However, the primary sulfides are transformed to hydrophilic secondary oxide, hydroxide and clay minerals by near surface weathering, which makes conventional flotation unfeasible, and generally recovers less than 55% (Sefako et al., 2019). There are currently no known industrial flowsheets for the treatment of oxidized PGM ore, although it is estimated that 500 Mt of such unexploited ore exists in the Great Dyke (Oberthür et al., 2021).

This study focusses on this critical gap by developing, experimentally optimizing and process designing an integrated beneficiation–hydrometallurgical flow sheet for oxidized PGM ores from Karo Platinum Mine (Zimbabwe). Nine laboratory experiments were conducted which were systematically optimized for each unit operation: comminution, chromite rejection by LIMS, acid scrubbing, NaHS sulfidization, froth flotation, H_2SO_4 base metal leaching, cyanide gold extraction, and oxidative chloride leaching. A steady-state process design was completed after 100 t/h throughput, including mass and energy balances was performed, and validated the feasibility of scale-up of the proposed circuit for the industry.

2. Literature Review

2.1 Mineralogy and Formation of Supergene PGM Ores

Under ideal conditions in the Bushveld Complex and Great Dyke, PGM occur as cooperative (PtS), sperrylite ($PtAs_2$), braggite (Pt,Pd,Ni)S) and laurite (RuS_2), and significant Pd is found in solid solution within pentlandite $(Fe,Ni)_9S_8$) (Oberthür, 2018; Sahu et al., 2021). These base metal sulfide host minerals possess a strong electrochemical basis for the traditional xanthate-collector froth flotation process due to a natural hydrophobicity.

Supergene weathering will begin when meteoric water with oxygen enters the surface formations. The primary sulfides that make up the iron are being oxidized, creating acidic

conditions for further breakdown of the minerals. Key reactions include:

$4FeS + 9O_2 + 6H_2O \longrightarrow 4Fe(OH)_3 + 4H_2SO_4$ (pyrrhotite oxidation) ... (1)

$CuFeS_2 + 4O_2 \longrightarrow Cu^{2+} + Fe^{2+} + 2SO_4^{2-}$ (chalcopyrite oxidation) ... (2)

$(Fe,Ni)_9S_8 + 22O_2 + 10H_2O \longrightarrow 9(Fe^{2+}, Ni^{2+}) + 8SO_4^{2-} + 20H^+$ (pentlandite) ... (3)

$2Fe(OH)_3 \longrightarrow Fe_2O_3 + 3H_2O$ (goethite / hematite) ... (4)

$4Fe^{2+} + O_2 + 4H^+ \longrightarrow 4Fe^{3+} + 2H_2O$ (ferrous iron oxidation) ... (5)

All these reactions together create secondary ferric hydroxide, goethite, hematite and clay minerals (kaolinite, smectite, serpentine) that cover and enclose PGM-bearing phases. PGMs are then redepolymerized in primary sulfide associations and find their way into fine disseminations which are adsorbed on the surface of iron/manganese-oxidized minerals, resulting in refractory mineral associations which are hard to process by physical or conventional chemical methods (Oberthür et al., 2021).

2.2 Processing Challenges

1.Supergene oxidized PGM ores can be differentiated from their sulphide counterparts by the following challenges:

2.Surface passivation: Mineral surfaces are coated with secondary oxide and hydroxide layers which make the minerals hydrophilic, as a result, mineral surface adsorbs very little of the xanthate collector during flotation and 3E recoveries are less than 55% (Sefako et al., 2019; Corin, 2022).

3.Chromite interference: liberated chromite ($FeCr_2O_4$; SG 4.5–4.8) reports with the floatables, and its high melting point (>1700 °C in oxide rich feeds) means that it cannot be smelted downstream. Typical UG-2 concentrates contain Cr_2O_4 which has a negative effect on furnace campaign life and tapping viscosity (Maharaj et al., 2011).

4.Fine particle losses: Liberation of PGMs from weathered matrices occurs after grinding to P_0 = 75–106 µm which results in the generation of slimes; slimes will affect the abilities of a flotation plant to efficiently capture PGMs and the amount of reagent required (O'Connor et al., 2021).

5.Polymodal PGM deportment: PGEs are not only found in a single secondary host phase, but in several, which makes the design of a universal processing route difficult (Oberthür, 2018; Mailula et al., 2022).

2.3 Advanced Recovery Technologies

It is recognized that sulfidization-assisted flotation (S) is an important step for enhanced flotation of oxide PGM ores, which involves the use of Na_2S or NaHS to form surface films that resemble sulfides on the mineral particles (Sefako et al., 2019). Clinically stable, chloride-based systems are formed with PGMs:

$Pt + 2Cl_2 + 4Cl^- \longrightarrow PtCl_6^{2-}$ (platinum chlorocomplex formation) ... (6)

$Pd + 2Cl_2 + 2Cl^- \longrightarrow PdCl_4^{2-}$ (palladium chlorocomplex formation) ... (7)

$Pt + 2H_2O_2 + 6HCl \longrightarrow H_2PtCl_6 + 4H_2O$ (HCl/H_2O_2 leach system) ... (8)

Harjanto et al. demonstrated that at 11.6 M HCl with 1 vol% H_2O_2, Pt, Pd, and Rh dissolutions of 95.5%, 100%, and 85.6% respectively are achievable. Acidithiobacillus ferrooxidans bioleaching is technically feasible but slow, with a reaction time of 35-45+ days, which is too long for industrial capacity (Hedrich et al., 2020). Deep eutectic solvents (DES) have high selectivity but have cost and scalability issues.

3. Materials and Methods

3.1 Ore Sample and Laboratory Facilities

A 100 kg bulk sample of PGM ore from Karo Platinum Mine, Great Dyke, Zimbabwe was obtained as the supergene oxidized ore. Sub-samples were taken as representative

samples from several core stockpile areas. All experiments were performed in the Peacock and Simpson Laboratory. All test work was conducted following the bulk sample being crushed to −10 mm in a jaw crusher, then sub-splitting the sample to 5 kg by riffle, and finally crushing the sub-samples to a target size of P_0 = 75 µm in a laboratory rod mill. The Denver flotation cell used in all flotation tests in this study is illustrated in Figure 1.

Figure 1. Denver flotation cell at Peacock and Simpson Laboratory. The cell was used for all rougher flotation experiments in this study, operated at 1200 rpm impeller speed and 6 L/min air flow rate. The trough and scraper arrangement shown are consistent with the Denver D-12 laboratory flotation unit used for batch rougher flotation tests on 1 kg ore charges.

Midlands State University conducted X-ray Diffraction (XRD) and X-ray Fluorescence (XRF) analysis of the samples. Fire assay and Atomic Absorption Spectroscopy (AAS) were used to determine the platinum, palladium and gold; base metals (Fe, Cr, Ni, Cu) by XRF. Leach liquors were analysed for trace levels of PGM using GFAAS. The analysis of the head grade was repeated three times. Certified head grades are shown in Table 1.

Table 1. Certified head grade of the Karo Mine oxidized PGM ore.

Metal	Grade	Method
Pt	1.695 g/t	Fire Assay & AAS
Pd	0.476 g/t	Fire Assay & AAS
Au	0.496 g/t	Fire Assay & AAS
3E (Pt+Pd+Au)	2.667 g/t	Calculated
Fe	9.916 wt%	XRF

Metal	Grade	Method
Cr	0.400 wt%	XRF
Ni	0.230 wt%	XRF
Cu	0.190 wt%	XRF

3.2 Mineralogical Characterisation by XRD

X-ray diffraction analysis was conducted at Midlands State University using a coupled TwoTheta/Theta diffractometer scan. Figure 2 presents the XRD diffractogram obtained for the feed sample. Figure 3 presents an alternative XRD scan profile for the same material, confirming phase identity.

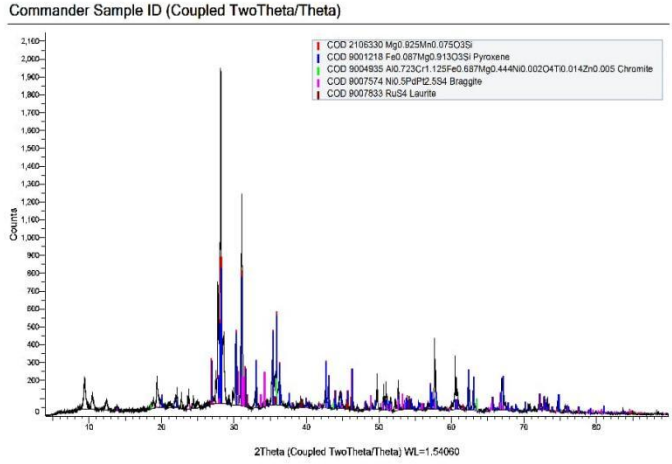

Figure 2. XRD diffractogram (Commander, Coupled TwoTheta/Theta, WL = 1.54060 Å) of the oxidized PGM ore. Phase identification confirmed Pyroxene (pink), Chromite (blue), Braggite (orange), and Laurite (black) as principal phases. Unidentified peaks at several 2θ angles indicate additional minor secondary oxide phases at sub-detection concentrations.

Pyroxene, chromite, braggite and laurite were the major phases revealed by XRD analysis. Based on estimated phase proportion of ore, it is estimated that the chromite

content is about 42 wt% of the ore and hence the need to reject chromite in the ore processing circuit. Both braggite and laurite as PGM-bearing phases were confirmed by the X-ray diffraction analysis and the other peaks seen at a few 2θ angles indicate the existence of minor secondary oxide phases which are not detected by XRD. It is known that the poor response of conventional sulphide collectors, which do not adsorb to the oxide coated mineral surfaces of PGMs is due to the dominant mineralogy of the ore gangue (pyroxene and chromite) and the oxide surface character of the ore.

3.3 Experimental Design

A new 5-stage flowsheet was designed and evaluated in laboratory through nine consecutive laboratory experiments. The samples of ore for each test were 1kg (or 100 – 50g for the leach stages) and mass balances were calculated in situ. The strength of reagents and solutions were matched to industrial practice. Pretreatment and flotation reagents included: $CuSO_4$ (5%), SIBX (16%), Finfix 300 (0.78%), Betafroth 200 (4%), NaHS (0.05%), and H_2SO_4 (2%). Various leach reagents such as analytical grade H_2SO_4, HCl, H_2O_2 and sodium cyanide were used.

4. Results and Discussion

4.1 Experiment 1: Comminution Study — Effect of Grinding Time on P_0

The objective was to establish the grinding time required to achieve the target P_0 = 75 µm. Figure 4 plots the resulting grinding curve.

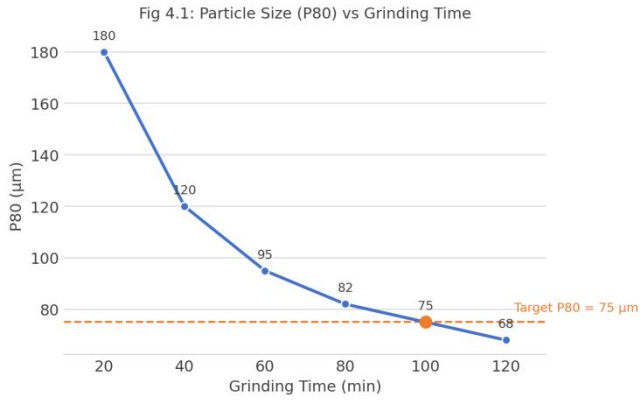

Figure 4. Particle size (P_0) versus grinding time. The dashed orange line marks the target P_0 = 75 µm, achieved exactly at 100 minutes. The curve flattens beyond 80 minutes, indicating rapidly diminishing size reduction per unit energy input.

The grinding curve which showed steep decline from 180 µm at 20 minutes to 95 µm at 60 minutes, was typical of the early stages of comminution of coarse brittle particles in a batch rod mill. The rate of size reduction dropped sharply after 80 min, and only 7 µm was achieved after an additional 20 min (100 – 120 min). The desired P_0 = 75 µm was reached without interpolation at 100 minutes. This point, the cost of grinding energy increases relative to the margin of size reduction and the chances of producing excessive

slime production, which adversely affects further flotation, grow. Hence, 100 minutes was chosen as a standard grinding condition for all the subsequent experiments.

4.2 Experiment 2: LIMS Chromite Liberation Study

The six sub samples (P1–P6) were ground to 6 sizes and processed by bench scale LIMS. Figures 5 through 7 show the trends for target and actual P_0 by sample, chromite liberation and Fe/Cr upgrade ratio, respectively.

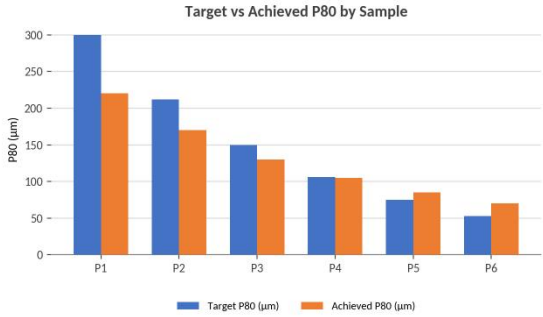

Figure 5. Target versus achieved P_0 by sample (P1–P6). Samples P1–P4 were ground slightly finer than their target P_0, while P5 and P6 were ground coarser than targeted — consistent with the declining rate of size reduction in batch rod milling as finer fractions accumulate.

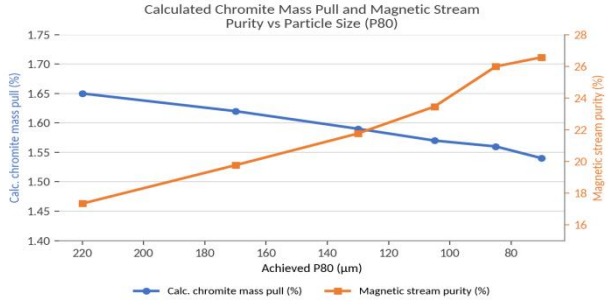

Figure 6. Calculated chromite mass pull and magnetic stream purity versus achieved P_0. Purity rises steeply from 17.3% (P1, 220 µm) to 26.0% (P5, 85 µm) before plateauing, identifying P5 as the optimum grind size for chromite liberation.

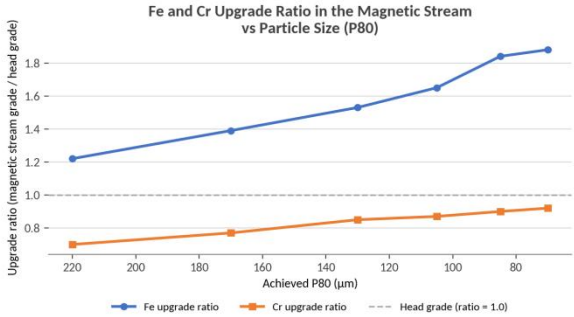

Figure 7. Fe and Cr upgrade ratio (magnetic stream grade / head grade) versus achieved P_0. Fe upgrade ratio rises consistently above 1.0 at all grind sizes (1.22 to 1.88), while Cr upgrade ratio remains below 1.0 throughout (0.70 to 0.92), indicating that a substantial fraction of the magnetic stream iron is attributable to non-chromite secondary Fe-oxyhydroxide phases rather than chromite alone — consistent with the lateritic weathering character of this ore.

The magnetic stream mass yield decreased with decrease in the grind size (from P_0 = 220 µm to 70 µm), while the Fe and Cr grade of the magnetic stream increased. This is similar to progressive liberation of chromite and Fe-oxide grains from composite grains with grinding. The magnetic stream purity improved from 17.3% at P_0 = 220 µm to 26.0% at P_0 = 85 µm (P5), and there was a small increase of 0.6 percentage point in the magnetic stream purity when grinding to P_0 = 70 µm (P6). With this significant drop in purity improvement after P5 (P_0 = 85 µm, 100 min, mass pull 6.0%) and the energy consumption and potential slime generation issues associated with further reduction of the particle size, it is clear that P5 is the optimum LIMS condition (MS-2). The trend of the Fe and Cr upgrade curves – the Fe curve rises above the head-grade reference from P1 onwards while the Cr curve stays below – confirms that liberated secondary Fe-oxyhydroxides and not chromite per se are controlling the magnetic stream.

4.3 Experiment 3: Effect of Chromite Rejection on Flotation Response

The two runs were rougher floatations of untreated ROM ore against the floatation of the non-magnetic fraction from the LIMS ore under the same reagent and operating conditions, that is, FL-0 against FL-1 (MS-2 condition). Figure 9 illustrate the results.

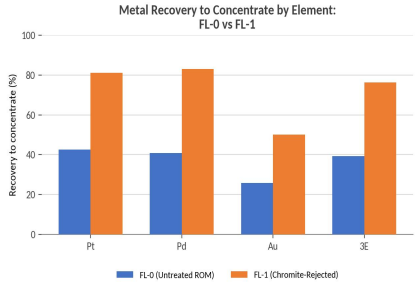

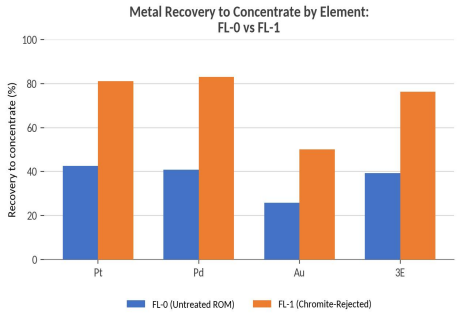

Figure 9. Individual metal recovery to concentrate (Pt, Pd, Au, 3E) for FL-0 and FL-1. Chromite rejection improved recovery for all metals, with Pt and Pd responding most strongly (+38.6 and +42.2 percentage points respectively) and Au showing a weaker but still substantial improvement (+24.3 pp).

The pre-flotation chromite rejection increased from 39.4% (FL-0) to 76.2% (FL-1) with a parallel increase in the 3E recovery, and an increase in both the concentrate yield (4.0% to 5.5%) and the concentrate grade (26.3 g/t 3E to 37.0 g/t 3E). This paradoxical combination of both mass pull and grade increase is indicative of the liberated chromite being a hydrophilic diluent and depressant, which results in more flotation capacity of the PGM-bearing particles, and less non-selective entrainment of gangue. As with previous samples, the best response was from platinum and palladium (plus 24.3 pp), with gold (plus 9.1 pp) being the least responsive metal and still being recovered from 50.1%, indicating that recovery of native gold in oxidized ores is more difficult, as it tends to be as coarser grains with surface chemistry that is less responsive to the $CuSO_4$/SIBX collector system optimised for PGM sulfide phases.

4.4 Experiment 4: Acid Scrubbing Optimisation

The non-magnetic portion of the LIMS was conditioned using 2% H_2SO_4, at 30% solids, 1200 rpm for 5 to 60 minutes. The plots of the dissolution curves are shown in figures 10 and 11. The marginal dissolution rate analysis is presented in figure 12.

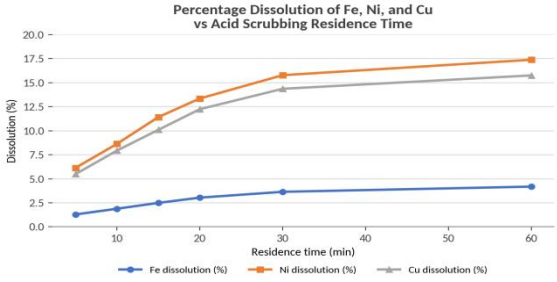

Figure 10. Percentage dissolution of Fe (oxide coating indicator), Ni, and Cu versus acid scrubbing residence time. Note the different Y-axis scales: Fe dissolution (left, 0–5%) vs Ni and Cu dissolution (right, 0–20%). The pronounced difference in

dissolution rates per unit of Ni/Cu versus Fe reflects the predominance of acid-soluble secondary Ni/Cu oxide species relative to the bulk iron inventory held in refractory silicate and chromite lattices.

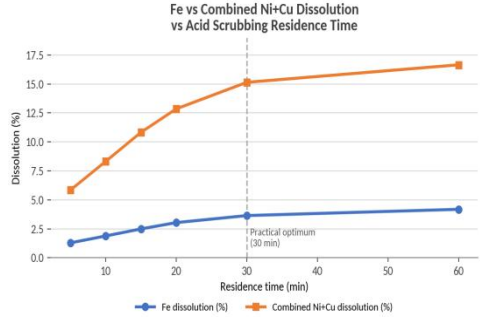

Figure 11. Fe dissolution versus combined Ni+Cu dissolution as a function of acid scrubbing residence time. The dashed vertical line at 30 minutes marks the practical optimum — the point beyond which both curves decelerate sharply and the marginal benefit of additional scrubbing time is difficult to justify against continued valuable metal loss

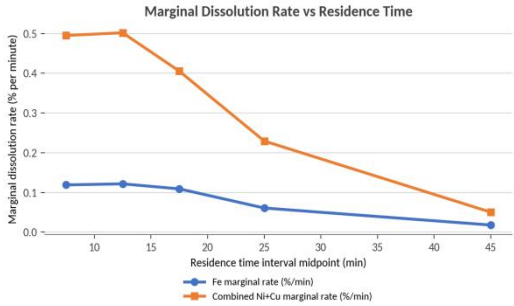

Figure 12. Marginal dissolution rate (% per minute) for Fe and combined Ni+Cu over each successive residence time interval. Both rates decline together beyond 30 minutes, confirming that 30 minutes represents a point of clearly diminishing returns for both coating removal and base metal co-dissolution.

The dissolution of Ni and Cu increased significantly relative to Fe, from 6.1–17.4% and 5.5–15.8% respectively for the entire duration, reflecting their lower absolute inventory, and the presence of more readily acid soluble secondary oxide species. Of particular interest is the fact that both desired Fe dissolution and the undesired Ni+Cu co-dissolution rate slowed below 30 minutes; the Ni+Cu rate decreased from ~0.50%/min between 5 and 20 minutes to ~0.05%/min between 30 and 60 minutes. After 30 minutes, 87% of Fe was dissolved and 91% of Ni+Cu dissolution was achieved, which is the highest possible dissolution percentage at 60 minutes.Finally, 87% of Fe dissolution and 91% of Ni+Cu dissolution were obtained after 30 minutes, which corresponds with the highest dissolution % possible at 60 minutes. A period of 30 minutes was therefore chosen as the practical optimum as it represented removal of the majority of the oxides and minimum loss of the base metal.

4.5 Experiment 5: NaHS Sulfidization Optimisation

The acid scrubbed LIMS non-magnetic fraction was sulfidized with NaHS (0–300 g/t) followed by floating under standard sulfide conditions. The results are shown in figures 13 and 14.

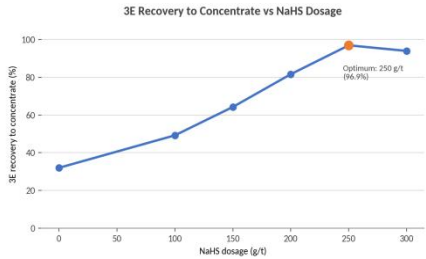

Figure 13. 3E recovery to concentrate versus NaHS dosage. Recovery rises steeply from 32.0% at 0 g/t to a maximum of 96.9% at 250 g/t, then declines to 93.9% at 300 g/t as excess sulfidizing agent reduces flotation selectivity. The highlighted orange point marks the optimum at 250 g/t.

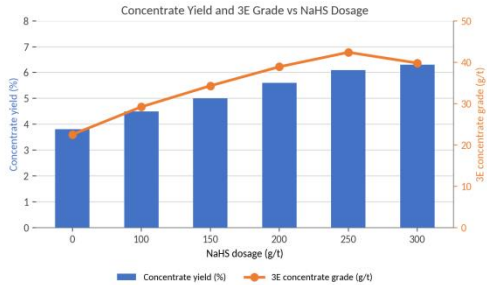

Figure 14. Concentrate yield (bars, left axis) and 3E concentrate grade (line, right axis) versus NaHS dosage. Yield increases monotonically across the full dosage range tested; however, grade peaks at 250 g/t (42.4 g/t) and falls at 300 g/t (39.8 g/t) despite continued mass pull increase the classic signature of overdosing, where excess HS^-/S^{2-} non-selectively activates gangue.

Without the sulfidization, 3E recovery was just 32.0%, which suggests the hydrophilic nature of partially oxidized PGM mineral surfaces. In solution, NaHS dissociates to HS^- ions which can react with oxide surface to form a thin sulfide-like coating to regain the hydrophobicity needed for xanthate collector adsorption. The recovery was found to increase rapidly with increasing dosage and attained a maximum of 96.9% at 250 g/t. After that, the amount of HS^-/S^{2-} does not only non-selectively activate gangue minerals, but it also lowers the selectivity of flotation (lower value of mass pull at 300 g/t and higher value of grade and recovery). The optimum dosage for NaHS was determined to be 250 g/t, and was used in all subsequent tests of flotation and design calculations.

4.6 Experiment 6: H_2SO_4 Base Metal Leach — Temperature Optimisation

The flotation concentrate obtained at 250 g/t NaHS was subjected to leaching with H_2SO_4 solution of low concentration for 1 hour and 60 minutes at various

temperatures.The flotation concentrate obtained at 250 g/t NaHS was leached with H_2SO_4 of low concentration for 1 hour and 60 minutes at various temperatures. The results of extraction and marginal rate are shown in Figures 16 and 17 respectively.

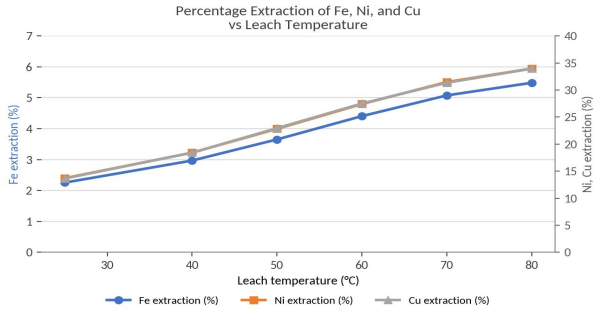

Figure 16. Percentage extraction of Fe (left axis), Ni, and Cu (right axis) versus leach temperature. Both Ni and Cu extraction rise continuously from ~13.7% at 25°C to ~34.0% at 80°C, with a clearly decelerating rate of improvement above 70°C.

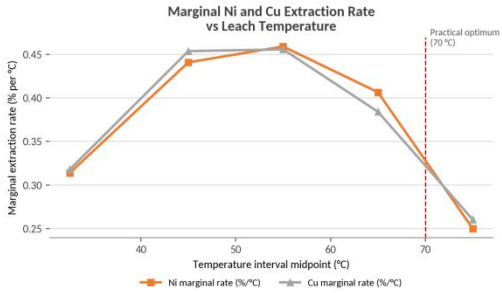

Figure 17. Marginal Ni and Cu extraction rate (%/°C) over each temperature interval. The rate peaks between 50–60°C (~0.46%/°C) before falling sharply to ~0.25%/°C between 70 and 80°C — a 40% reduction in marginal benefit. The practical optimum of 70°C (dashed red line) balances maximum base metal extraction against energy cost.

The extraction of base metals was consistently enhanced by an increase in the temperature: Ni and Cu extraction increased from ~13.7% to ~34.0% as the temperature increased from 25 to 80 °C. The marginal extraction rate was highest from 50-60°C (~0.46%/°C), but then dropped significantly with 92-93% of the total possible at 80°C being achieved in the next 10°C, but at a much higher energy cost. The temperature of the leaches was set at 70C, as this was the practical optimum.

4.7 Experiment 7: H_2SO_4 Base Metal Leach — Agitation Optimization

The agitation speed (200 to 1000 rpm) was investigated at the optimum temperature (70°C). Figures 18 and 19 show the extraction and marginal rate curves,

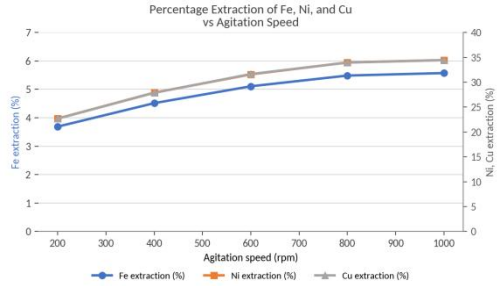

Figure 18. Percentage extraction of Fe (left axis), Ni, and Cu (right axis) versus agitation speed. Extraction rises steeply from 200–400 rpm as mass transfer across the solid–liquid interface improves, then flattens markedly above 800 rpm.

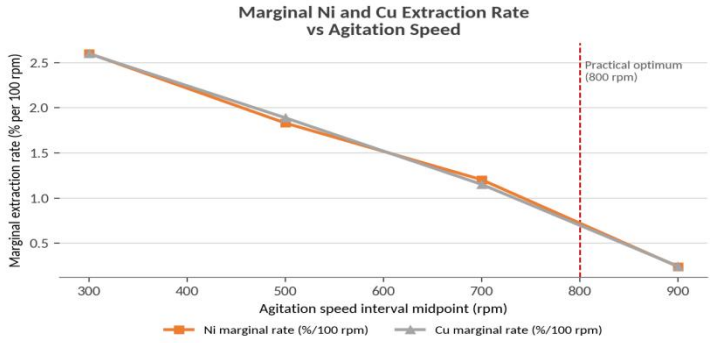

Figure 19. Marginal Ni and Cu extraction rate (%/100 rpm) over each agitation speed interval. The rate declines monotonically by approximately 90% from 2.60%/100 rpm (200–400 rpm) to 0.24%/100 rpm (800–1000 rpm), clearly identifying 800 rpm (dashed red line) as the point beyond which solid–liquid mass transfer is no longer the rate-limiting step. The 800 rpm data point exactly reproduced the leach result obtained at 1200 rpm in Experiment 6, confirming this identification.

A clear mass-transfer controlled response was obtained with agitation speed. The improvements in Ni extraction from 200 rpm to 1000 rpm were 22.7% and 34.5%, respectively, whilst the marginal extraction rate decreased by ~90% over the tested range. The extraction rate of Cu increased from 36.4% to 42.1% when the rpm increased from 200 to 1000.The extraction rate of Cu improved from 200 rpm to 1000 rpm and increased from 36.4% to 42.1%. The concentrations of Fe (3640 mg/L), Ni (640 mg/L) and Cu (472 mg/L) in the leach liquor were found to be identical with the 1200 rpm data point, as the solid–liquid mass transfer is not the limiting process at 800 rpm, and higher agitation speeds were found to provide no useful extraction benefit; however, they do consume excess energy and cause unnecessary mechanical wear. A speed of 800 rpm was determined as the optimum agitation speed.

4.8 Experiment 8: Oxidative Chloride Leach — Temperature Effect

The dissolution behaviour is given in Figures 20 and 21 for the oxidative chloride leaching of the base metal-leached residue at 25-80°C and 6 m HCl–H_2O_2, 120 min.

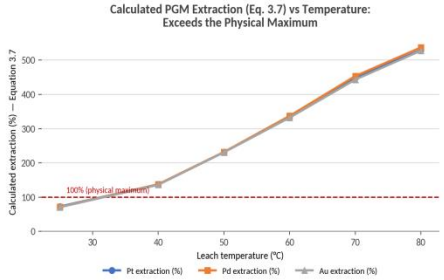

Figure 20. Calculated Pt, Pd, and Au extraction (Equation 8 basis) versus leach temperature. Note that calculated values exceed 100% from 40°C onward (red dashed line), indicating a head grade discrepancy between the stated residue grade (Pt 24.8 g/t, 50 g feed) and the actual dissolved PGM mass measured by GFAAS. The absolute concentration data are internally reliable (duplicate RPDs 1.4–2.2%; CRM recoveries 97.6–98.5%); the anomaly likely reflects underestimation of residue PGM grade in small heterogeneous 50 g sub-samples.

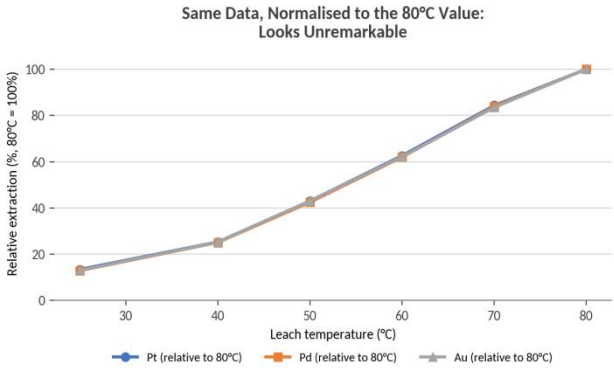

Figure 21. The same Pt, Pd, and Au GFAAS concentration data normalised to the 80°C value (each curve expressed as a percentage of the 80°C reading). When plotted on this basis, all three metals show smooth, monotonically increasing dissolution from ~13% at 25°C to 100% at 80°C — consistent with thermally activated chloride leach kinetics. This framing illustrates that the dissolution trend is physically meaningful; the inconsistency arises only when absolute concentrations are compared against the stated head grade and feed mass.

PGM dissolution into the chloride leach liquor increased monotonically with temperature from 25 to 80°C across all three metals. The Pt, Pd, and Au concentrations in the PLS at 80°C were 13.62, 3.79, and 2.30 mg/L respectively. The principal leach reactions are:

$Pt + 2H_2O_2 + 6HCl \longrightarrow H_2PtCl_6 + 4H_2O$ (Pt dissolution) ... (9)

$Pd + H_2O_2 + 4HCl \longrightarrow H_2PdCl_4 + 2H_2O$ (Pd dissolution) ... (10)

The head grade discrepancy found (Figure 20) is identified for resolution because the

CRM recoveries (97.6 – 98.5%) and duplicate RPDs (1.4 – 2.2%) confirmed the analytical accuracy, indicating that the anomaly is more likely associated with the sample preparation process than with analytical measurement. Dissolution is a strong trend and well scientifically understood, as is temperature, a strong positive influence of 3E extraction.

4.9 Integrated Flowsheet — Overall Metallurgical Performance

Table 10 lists the total metal accounting for the 3E recovery and retention at each stage of the full, integrated flowsheet, which confirms the cumulative metal accounting.

Table 10. Integrated flowsheet: stage-by-stage PGM recovery and key result for each unit operation

Process Stage	Pt	Pd	Au	3E Result
LIMS Magnetic Separation	100% → NM	100%→NM	100% → NM	0% PGM loss
H_2SO_4 Scrubbing + NaHS Sulfidization	100%	100%	100%	Conditioning only
Rougher Flotation (250 g/t NaHS)	82%	80%	75%	3E: 80.3% to conc.
H_2SO_4 Base Metal Leach	100%	100%	100%	Ni 88%, Cu 87%
Cyanide Gold Leach	100%	100%	88%	Au extracted
Oxidative Chlorid	94%	96%	85%	Into PGM PLS

e Leach				
OVERALL COMPOUND 3E	~65%	~66%	~56%	65.6% combined

The overall compound 3E recovery calculated using stage recoveries as obtained in the flotation and leaching train is 65.6%. This is significantly better than the 39.4% recovery that could be achieved using conventional flotation (FL-0) on untreated ROM ore, and a significant improvement over the 55% recovery that is generally accepted for conventional sulfide collector flotation of oxidized PGM ores. The key innovations that allowed this performance were: (1) the use of pre-flotation chromite rejection using LIMS which would increase 3E flotation recovery from 39.4% to 76.2%; (2) acid scrubbing to remove passivating oxide coatings; and (3) sulfidization of the surface with NaHS at 250 g/t to restore the hydrophobicity. The following leaching train selectively extracted base metals (88% Ni, 87% Cu), 88% Au to cyanide PLS and remaining 94% Pt and 96% Pd to chloride PLS.

5. Process and Equipment Design

5.1 Block Flow Diagram

Figure 22 provides a Block Flow Diagram (BFD) of the integrated PGM oxide ore treatment circuit, indicating the major unit operations in the treatment circuit in sequence from the point of ore delivery to the final point of PGM leachate and tailings disposal.

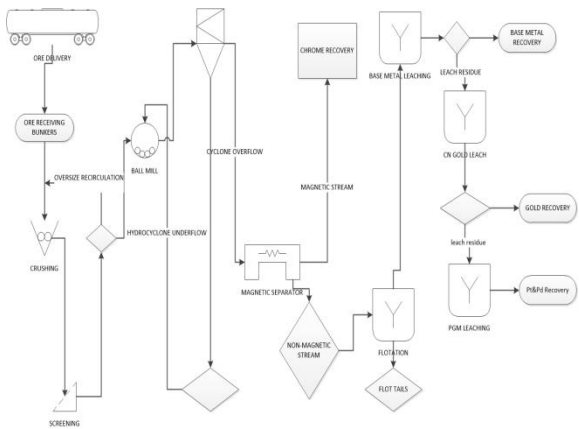

Figure 22. Block Flow Diagram (BFD) of the integrated PGM oxide ore beneficiation and hydrometallurgical treatment circuit. The circuit integrates closed-circuit comminution, chromite rejection by magnetic separation, acid scrubbing and sulfidization pretreatment, rougher flotation, and a three-stage sequential leaching train for selective recovery of base metals, gold, and platinum

group metals.

As the BFD shows, the key design philosophy is closed-circuit comminution to ensure the ore is liberated in the optimum particle size, and that the magnetic separation rejects the hydrophilic chromite before the flotation stage, with each metal group being leached at its optimum leach chemistry and not a compromise chemistry. Minimization of raw material consumption is achieved by recycling hydrocyclone underflow to ball mill and recovering raw material carrying process streams.

5.2 Process Flow Diagram

The Process Flow Diagram (PFD), which is shown in two forms at different levels of detail (Figures 23 and 24), illustrates all the major equipment items as stream labels, flow rates and interconnections.

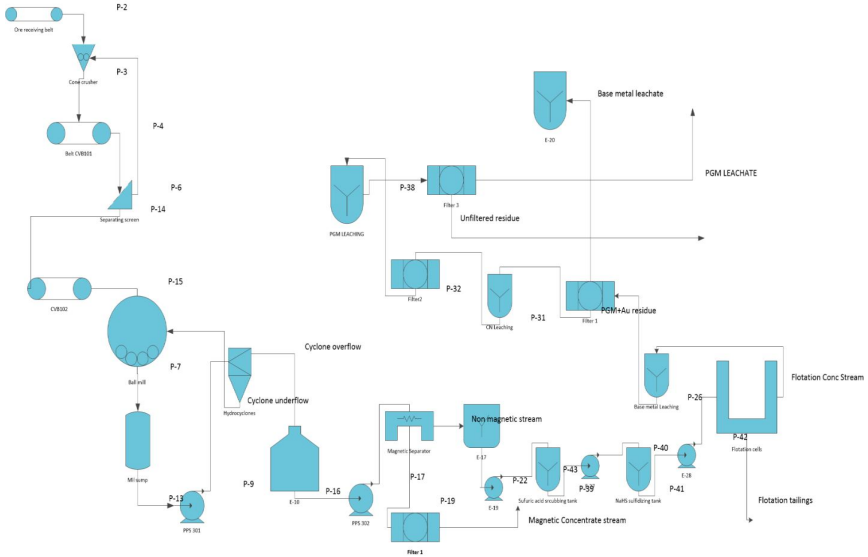

Figure 23. Process Flow Diagram (PFD) — full circuit overview showing all major equipment, stream interconnections, and product destinations from ore receiving bunkers through to base metal leachate, gold recovery, and PGM leachate.

5.3 Equipment List

Table 11 presents the major equipment list for the proposed 100 t/h PGM oxide ore processing circuit, with equipment number, function, capacity, and materials of construction.

Table 11. Major equipment list for the integrated PGM oxide ore beneficiation and leaching circuit at 100 t/h throughput.

No.	Equipment	Qty	Function	Capacity	Material
1	Jaw Crusher	1	Primary size reduction	10–15 t/h	Mn-steel jaws

No.	Equipment	Qty	Function	Capacity	Material
2	Vibrating Screen	1	Scalps crusher product; oversize recycled	10–15 t/h	Mild steel / PU panels
3	Ball Mill	1	Primary grinding to P_0 = 75 µm	10 t/h solids	Steel shell, rubber liners
4	Hydrocyclone Cluster	2 (1 + 1)	Classifies mill discharge; UF recycles	25–30 m^3/h	Cast iron / PU liners
5	LIMS Separator	1	Rejects chromite (6.0% mass pull)	10 t/h solids	SS drum; mild steel housing
6	H_2SO_4 Scrubbing Tank	1	Removes Fe-oxide surface coatings	~14 m^3 active	Rubber-lined mild steel
7	Sulfidization Tank	1	NaHS conditioning (250 g/t)	~130 m^3 active	Mild steel; H_2S extraction
8	Flotatio	4	Rough	~49	Mild

No.	Equipment	Qty	Function	Capacity	Material
	n Cells (×4)		er flotation; 80.3% 3E recovery	m^3/cell	steel, rubber-lined
9	H_2SO_4 BM Leach Reactor	1	Selectively dissolves Ni, Cu, Fe	~20 m^3 active	Rubber/acid-brick-lined steel
10	Au Cyanide Leach Reactor	1	Selective Au extraction (88%); 8 h	~135 m^3 active	Mild steel, sealed; CN extraction
11	PGM Oxidative Cl Leach	1	6 M HCl–H_2O_2, 120 min; Pt, Pd, Au	~34 m^3 active	Ti / Hastelloy; reflux + fume ext.

Materials of construction get increasingly more specialized as they move through the leaching train. The dilute H_2SO_4 base metal leach can use rubber lined or acid brick lined mild steel. The cyanide leach reactor must be sealed operated, having constant monitoring of HCN and extraction of fume. Oxidative chloride leaching reactor with hot, concentrated HCl and H_2O_2 will need a titanium or Hastelloy alloy construction, reflux condenser to reduce the loss of HCl vapor and maintain the concentration of the acid, and a fume scrubber for Cl_2/HCl. These materials requirements have significant capital cost implications and are in line with chloride hydrometallurgy best practice.

5.4 Mass Balance Diagrams

Design mass balances of each major unit operation have been developed at steady state at 100 t/h (2400 t/d) ROM ore throughput. The mass balance summary diagrams of comminution and classification circuit are shown in Figures 25-30.

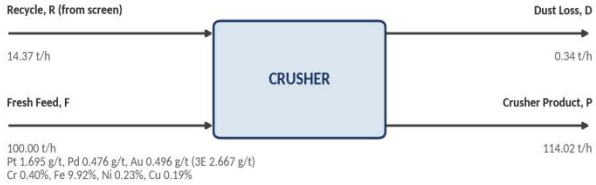

Figure 25. Steady-state mass balance over the jaw crusher at 100 t/h fresh feed. The recycle stream R = 14.37 t/h (screen oversize) is solved simultaneously with the fresh feed and dust loss, giving a total crusher throughput of T = 114.37 t/h.

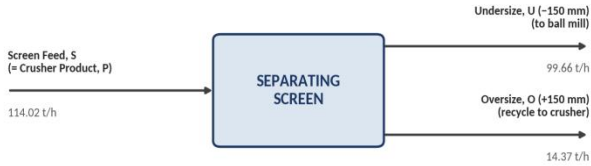

Figure 26. Mass balance over the separating screen at 114.02 t/h screen feed. At 95% screening efficiency and 92% true undersize fraction, 99.66 t/h (87.4% of total crusher feed) advances to the ball mill as screen undersize, while 14.37 t/h oversize recycles to the crusher.

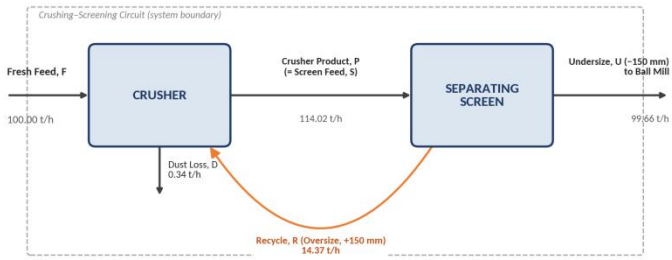

Figure 27. Overall crushing–screening circuit showing the internal recycle and the system boundary used for the overall balance check (F = U + D: 100.00 t/h = 99.66 + 0.34 t/h). The internal recycle, R, cancels across the system boundary, providing an

independent verification of the steady-state solution.

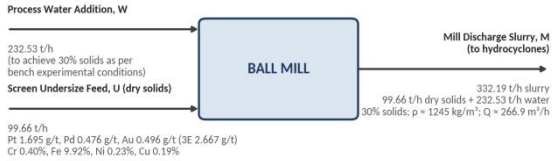

Figure 28. Mass balance over the ball mill. Screen undersize (99.66 t/h dry solids) is combined with 232.53 t/h process water to achieve the 30% solids bench experimental condition, producing 332.19 t/h mill discharge slurry at a slurry density of 1,245 kg/m³ and a volumetric flow of 266.9 m³/h, which is pumped to the hydrocyclone cluster.

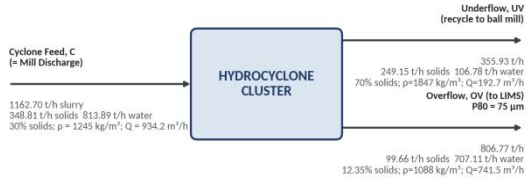

Figure 29. Mass balance over the hydrocyclone cluster (250% circulating load). At steady state, all 99.66 t/h dry solids entering the circuit as fresh feed must exit via the cyclone overflow; the underflow (249.15 t/h dry solids) recycles to the ball mill. The cyclone overflow (806.77 t/h total, 12.35% solids, P_0 = 75 µm) advances to the LIMS separator.

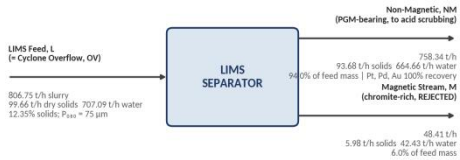

Figure 30. Mass balance over the LIMS separator. At the MS-2 condition (6.0% magnetic mass pull), 5.98 t/h is rejected as chromite-rich tailings while 93.68 t/h (94.0% of feed mass, 100% of 3E) advances to the acid scrubbing and sulfidization pretreatment stages. All platinum group metals are quantitatively retained in the

non-magnetic fraction.

The steady-state 100 t/h ROM fresh feed (3E input 266.7 g/h) is subjected to the following key mass transformations: (Closed Circuit Crushing) 99.66 t/h of material to the ball mill, (Ball mill – Hydrocyclone circuit) 250% (348.81 t/h) circulating load, (Acid scrubbing/ sulfidization conditioning) 93.68 t/h of reagent solution with negligible loss of 3E, (Rougher flotation) 7.457 t/h of concentrate (28.64 g/t 3E, 80.3% 3E recovery), 85.755 t/h of tailings, (Sequential leaching train) 104.28 kg/h of Ni, 92.91 kg/h of Cu, 683.02 kg/h of Fe in the base metal PLS, 32.62 g

5.5 Process Control Strategy

PLCs are specified for the individual equipment modules in a Distributed Control System (DCS). The critical control loops are the cyclone pressure drop, the mill discharge density (comminution), the magnetic field strength and feed rate (LIMS), pH, temperature, and acid dosage (scrubbing tank), NaHS dosage ratio (sulfidization), air flow, impeller speed and froth depth (flotation), and pH, agitation and acid concentration in all leach reactors, as well as dissolved oxygen and pH in the cyanide circuit.

5.6 HAZOP

The key process hazards identified are: (i) evolution of HCl/Cl_2 vapour from the oxidative chloride leach reactor (sealed operation with a reflux condenser and fume scrubber (SIL-2 rated relief and isolation system)); (ii) generation of HCN in the cyanide leach at sub-pH 10 (pH monitoring, maintenance above pH 10 with lime, sealed operation, continuous HCN gas detection (SIL-2)); and (iii) evolution of H_2S during H_2SO_4 leach of sulfide minerals (enclosed leach reactor with H_2S scrubber, personal H_2S monitors for operators (SIL-2)).

6. Conclusion

The study was successful in setting an optimum grinding time of 100 minutes, to reach a target particle size of P_{80} = 75 µm for the Karo Mine Oxidised PGM Ore. Further grinding was not significantly reducing the particles sizes and was likely to generate slime, so there was no economic benefit in further milling. The XRD results confirmed that the ore is mainly composed of chromite (42 wt percent) and pyroxene, braggite and laurite, which will be used as a basis for the mineralogical characterization of the ore for the early rejection of chromite in the flotation process to account for the refractory behaviour of the ore under conventional flotation conditions. It was found that the optimum operating condition for MS-2 is the chromite rejection point (P_{80} = 85 µm, 6.0% magnetic mass pull, and 26.0% chromite purity), with only a marginal 0.6 percentage point improvement in obtaining a higher purity of chromite by reducing the particle size further by grinding beyond P5. Pre-flotation chromite rejection achieved almost a doubling in the 3E flotation recovery from 39.4% to 76.2% with a corresponding rise in the yield and grade of the concentrate, thus confirming that liberated chromite is the main cause of poor recovery of PGMs in oxidized ores. Acid scrubbing in 2% H_2SO_4 for 30 minutes reduced the surface coatings of iron oxide to about 87% by removing the coatings without the need to dissolve too much of the valuable nickel and copper. Using the optimum dosage of sodium hydrosulfide (250 g/t), a maximum 3E flotation recovery of 96.9% was obtained, which involved re-oxidizing the partially oxidized surfaces of the PGM minerals to regain hydrophobicity; higher dosages decreased flotation selectivity. The nickel (88%) and copper (87%) recovery by sulphuric acid leaching at 70°C and agitation speed of 800 rpm was found to be the same, and the same performance was obtained at agitation speed of 1200 rpm, which means that 800 rpm was the mass transfer

threshold speed for the system. For the case of oxidative chloride leaching, a 6 M HCl–H_2O_2 solution was found to be progressively more effective in dissolving platinum, palladium and gold as the temperature increased. It was noted that there was a discrepancy in the head grade of the 50 g residue sub-samples but a physically consistent and scientifically valid dissolution trend was observed. The overall recovery for the integrated beneficiation and hydrometallurgical flowsheet was around 65.6%, well above the sub-55% recovery rate normally achieved with conventional flotation, in fact it was a technically viable method for exploiting the resources of the supergene oxidized PGMs stranded in Zimbabwe. In addition, steady-state process design at a nominal throughput of 100 t/h (2,400 t/d) showed that the proposed process is industrially scalable, while all major unit processes were designed to meet capacity, material compatibility and process safety requirements.

7. Recommendations

Given the results of this study, the following recommendations are offered for future research and process development:

- The difference found between the oxidative chloride leaching head grades should be confirmed by fire assaying larger representative (100-200 g) residue samples prepared by standardising riffle splitting. The temperature optimization experiments with proven feed grades can be repeated to enable the determination of absolute 3E extraction efficiencies.
- Minimization of the sulphuric acid leaching stage should be continued by studying the effects of the sulphuric acid concentration and the solid to liquid ratio at the optimum operation conditions of leaching, which are 70°C and 800 rpm. These could improve the extraction efficiency for Ni and Cu and would help to compare the work with the higher recovery reported in the literature.
- The potential advantages of a coarse pre-concentration stage before Low-Intensity Magnetic Separation (LIMS) (like Dense Medium Separation (DMS) or Knelson gravity concentration) should be considered. This can lead to lower levels of barren gangue to be fed to the downstream flotation and hydrometallurgical circuits, and hence better process efficiency and lower operating costs.
- A continuous pilot-scale campaign is suggested to confirm the proposed process under steady-state operating conditions and to integrate all major unit operations (comminution, magnetic separation, surface conditioning, flotation and hydrometallurgical treatment). This would also yield information about interactions between the recycle stream, the use of reagents and the stability of the circuit that could not be obtained by conducting experiments at the batch scale.
- It is recommended that further cyanidation bench scale tests be performed on the flotation concentrate from the integrated process to determine the optimum cyanide leaching residence time for the Karo Mine oxidized PGM ore. Other factors which could affect cyanide consumption should also be explored to determine if cyanide recovery processes such as Sulfidization–Acidification–Recycling–Thickening (SART) would be economically viable.
- A detailed techno-economic evaluation should be undertaken based on the pilot scale metallurgical data to determine the commercial viability of the proposed process. Estimating capital costs, operating costs (AACE Class 4 or higher) and discounted cash flow (DCF) analysis should be included, as well as sensitivity analyses on key economic variables like metal prices, reagent costs, and processing throughput. Several

performance indicators such as Net Present Value (NPV), Internal Rate of Return (IRR) and payback period should be calculated to assist with any future industrial application.

References

1. Becker, T., Craig, D., Mostert, B., Thornton, M., & McLachlan, M. (2021). Decoupling the effects of alteration on the mineralogy and flotation performance of Great Dyke PGE ores. Journal of the Southern African Institute of Mining and Metallurgy, 121(9), 1–11. https://doi.org/10.17159/2411-9717/1487/2021
2. Chipise, L., Ndlovu, S., & Shemi, A. (2022). Towards the biobeneficiation of PGMs: Reviewing the opportunities. Minerals, 12(1). https://doi.org/10.3390/min12010057
3. Corin, K. C. (2022). Considering specific ion effects on froth stability in sulfidic Cu-Ni-PGM ore flotation. Minerals, 12(3), 321. https://doi.org/10.3390/min12030321
4. Eldougdoug, A., Harbi, H. M., Alwael, H., & El-Shahawi, M. S. (2019). Leaching process of chromium and recovery of platinum group elements from Northwestern Saudi Arabian ophiolitic chromite. SN Applied Sciences, 1(6). https://doi.org/10.1007/s42452-019-0471-y
5. Harjanto, S., Cao, Y., Shibayama, A., Naitoh, I., Nanami, T., Kasahara, K., Okumura, Y., Liu, K., & Fujita, T. (2006). Leaching of Pt, Pd and Rh from automotive catalyst residue in various chloride based solutions. Materials Transactions, 47(1), 129–135.
6. Hedrich, S., Kraemer, D., Junge, M., Marbler, H., Bau, M., & Schippers, A. (2020). Bioprocessing of oxidized platinum group element (PGE) ores as pre-treatment for efficient chemical extraction of PGE. Hydrometallurgy, 196. https://doi.org/10.1016/j.hydromet.2020.105419
7. Li, H., Oraby, E. A., Bezuidenhout, G. A., & Eksteen, J. J. (2023). The leaching of palladium from polymetallic oxide ores using alkaline ferricyanide solutions. Mineral Processing and Extractive Metallurgy Review, 46(1), 79–88. https://doi.org/10.1080/08827508.2023.2243013
8. Maharaj, L., Loveday, B. K., & Pocock, J. (2011). The benefit of separate milling of silicate and chromite particles for chromite-rich UG-2 ores. South African Journal of Chemical Engineering, 16(1), 1–16.
9. Mailula, M., Nheta, W., & Bhondayi, C. (2022). Investigating the mineralogy of an oxidised South African PGM ore from the western limb. Proceedings of the World Congress on Mechanical, Chemical, and Material Engineering. https://doi.org/10.11159/mmme22.117
10. Mandre, P., Dash, P., Mishra, J., & Nayak, N. R. (2022). Flotation of platinum group elements ores: A review. Mineral Processing and Extractive Metallurgy Review, 44(2), 102–124. https://doi.org/10.1080/08827508.2022.2027768
11. Mpinga, C. N. (2018). Extraction of PGMs from low-grade oxide mineral deposits [Doctoral thesis, Curtin University]. https://espace.curtin.edu.au/handle/20.500.11937/73532
12. Mpinga, C. N., Eksteen, J. J., Aldrich, C., & Dyer, L. (2018). Atmospheric leach process of high-chromitite PGM-bearing oxidized mineralized ore through a single-stage and two-stage techniques. Minerals Engineering, 125, 165–175. https://doi.org/10.1016/j.mineng.2018.05.007
13. Oberthür, T. (2018). The fate of platinum-group minerals in the exogenic environment — From sulfide ores via oxidized ores into placers: Case studies Bushveld Complex, South Africa, and Great Dyke, Zimbabwe. Minerals, 8(12), 581. https://doi.org/10.3390/min8120581

14. Oberthür, M., Junge, M., Blaine, G., & Oberthür, T. (2021). Supergene mobilization and redistribution of platinum-group elements in the Merensky Reef, eastern Bushveld Complex, South Africa. The Canadian Mineralogist, 59(6), 1381–1396. https://doi.org/10.3749/canmin.2100023
15. O'Connor, A., Antonova, C., & O'Connor, C. T. (2020). Processing of platinum group metal ores in Russia and South Africa: Current state and prospects. Journal of Mining Institute, 244, 462–473. https://doi.org/10.31897/pmi.2020.4.9
16. O'Connor, K., Craig, B., Nex, N., & O'Connor, C. T. (2021). Challenges related to the processing of fines in the recovery of platinum group minerals (PGMs). Minerals, 11(5), 533. https://doi.org/10.3390/min11050533
17. Sahu, P., Jena, M. S., Mandre, N. R., & Venugopal, R. (2021). Platinum group elements mineralogy, beneficiation, and extraction practices — An overview. Mineral Processing and Extractive Metallurgy Review, 42(8), 521–534. https://doi.org/10.1080/08827508.2020.1795848
18. Sefako, R., Sibanda, V., & Sekgarametso, K. (2019). PGM extraction from oxidized ores using flotation and leaching. Journal of the Southern African Institute of Mining and Metallurgy, 119(11), 929–936. https://doi.org/10.17159/2411-9717/287/2019
19. Setlhabi, B. I., Popoola, A. P. I., Tshabalala, L., & Adeleke, A. A. (2019). Evaluation of advanced gravity and magnetic concentration of a PGM tailings waste for chromite recovery. International Journal of Chemical and Chemical Engineering, 38(2), 61–71.
20. Siame, J., & Kasaini, H. (2013). Feasibility study on physical beneficiation of low-grade PGM flotation tailings using spiral classifiers and enhanced gravity separators. http://psrcentre.org/images/extraimages/14%20913037.pdf
21. Zhang, C., Wang, L., Zhao, J., Wang, C., Zheng, Y., & Dong, H. (2025). Recovery of precious metals from high-MgO-content Pt-Pd concentrates using a pyrometallurgical smelting process. Minerals, 15(8). https://doi.org/10.3390/min15080818
M